Supporting Information

Nanoparticles with Embedded Porphyrin Photosensitizers for Photooxidation Reactions and Continuous Oxygen Sensing

*Pavel Kubát,[†] Petr Henke,[‡] Veronika Berzediová,[‡] Miroslav Štěpánek,[‡] Kamil Lang[$] and Jiří Mosinger[‡$]**

[†]J. Heyrovský Institute of Physical Chemistry of the Czech Academy of Sciences, v.v.i., Dolejškova 3, 182 23 Prague 8, Czech Republic

[‡]Faculty of Science, Charles University, 2030 Hlavova, 128 43 Prague 2, Czech Republic

[$]Institute of Inorganic Chemistry of the Czech Academy of Sciences, v.v.i., 250 68 Řež, Czech Republic

Corresponding Author

* E-mail address: mosinger@natur.cuni.cz

Content

Experimental details		S-3
Figure S1	Light scattering measurements	S-5
Figure S2	Normalized UV-Vis spectra of **TPP-NPs**	S-5
Figure S3	Normalized UV-Vis spectra of **TMPyP-NPs**	S-6
Figure S4	Fluorescence emission spectra of **TPP-NPs**	S-6
Figure S5	Fluorescence emission spectra of **TMPyP-NPs**	S-7
Figure S6	Photostability test	S-7
Figure S7	Kinetics of $O_2(^1\Delta_g)$ photogenerated by **TPP-NPs** and **TMPyP-NPs**	S-8
Figure S8	Kinetics of the triplet states of TMPyP dissolved in H_2O	S-8
Figure S9	Kinetics of the triplet states of **TPP-NPs** in H_2O	S-8
Figure S10	Kinetics of the triplet states of **TMPyP-NPs** in H_2O	S-9
Figure S11	Kinetics of $O_2(^1\Delta_g)$, TPP triplet states and SODF of **TPP-NPs**	S-9
Figure S12	SODF of **TMPyP-NPs** and **TPP-NPs** in the presence of NaN_3	S-10
Figure S13	Temperature dependence of $O_2(^1\Delta_g)$ and TPP triplet state kinetics in the polystyrene nanofiber material	S-10
Figure S14	Dependence of SODF on oxygen concentration	S-11
Figure S15	Photooxidation of uric acid by the **TPP-NPs** or **TMPyP-NPs** dispersions containing the same number of NPs	S-12
Figure S16	Photooxidation of uric acid by the **TPP-NPs** or **TMPyP-NPs** dispersions containing the same content of TPP	S-12
Table S1	Parameters of prepared sulfonated NPs	S-13
Table S2	Parameters of prepared photoactive NPs	S-14
Table S3	Oxygen properties	S-15

Experimental details

Photophysical measurements. The measurements were performed in a 10 mm quartz cell placed inside a thermostatically-controlled holder that was heated or cooled using the Peltier effect to maintain temperature stability to within 0.1 °C. A piece of the nanofiber material was placed on a quartz plate and inserted in a quartz cell with H_2O. The samples were saturated by argon for the measurement in oxygen-free conditions. All samples were excited by a Lambda Physik FL 3002 dye laser (425 nm, pulse width 28 ns).

The triplet state kinetics were recorded by transient absorption spectroscopy at 460 - 500 nm using a 150 W Xe lamp (Phillips) equipped with a pulse unit and a R928 photomultiplier (Hamamatsu) using a laser kinetic spectrometer LKS 20 (Applied Photophysics, UK).

Time-resolved near-infrared phosphorescence of $O_2(^1\Delta_g)$ at 1270 nm was observed at a right angle to the excitation pulse using a homemade detector unit (interference filter, Ge diode Judson J16-8SP-R05M-HS). All measurements were performed in air atmosphere or in air-saturated solutions. Singlet oxygen-sensitized delayed fluorescence (SODF) was monitored at 650 nm (i.e., at the maximum of the fluorescence emission band) on the laser kinetic spectrometer LKS 20 (Applied Photophysics). The signals of both SODF and $O_2(^1\Delta_g)$ were averaged and were calculated as the differences between signals in air-saturated solutions and detector responses in argon-saturated solutions. The initial part of the signals fails due to light scattering and strong prompt porphyrin fluorescence, and they were omitted in all figures.

Light scattering measurements. The scattering intensities $I(t,q)$, were acquired for the scattering vector magnitudes, $q=(4\pi n_0/\lambda)\sin(\theta/2)$ (n_0 is the solvent refractive index), from 10.1 μm^{-1} to 25.5 μm^{-1} corresponding to the scattering angles θ from 45° to 150°. Each measurement took 10 s and provided the time-averaged scattering intensities, $I(q)=\langle I(t,q)\rangle$, and the normalized autocorrelation functions of the scattered light intensity, $g^{(2)}(\tau,q)=\langle I(t,q)I(t+\tau,q)\rangle/I^2(q)$. The $I(q)$ values were recalculated to the absolute scale using calibration by the toluene standard.

The static scattering data (Figure S1, curve 1) were fitted by the Guinier formula, $I(q)=I(0)\exp(-R_g^2q^2/3)$, to obtain the gyration radius of NPs, R_g = 42 nm, and the forward scattering intensity, $I(0)$. The latter value provided the molar mass of the NPs as

$$M_w = \frac{\lambda^4 N_A}{4\pi^2 n_0^2 (dn/dc)^2}\frac{I(0)-I_0}{c} = 6.8\times10^7 \text{ g mol}^{-1}, \quad \text{(S1)}$$

where N_A is the Avogadro constant, I_0 is the scattering from the solvent and $(dn/dc) = 0.27$ ml g^{-1} is the refractive index increment for polystyrene in water.

The autocorrelation functions were fitted using the second-order cumulant expansion,

$$g^{(2)}(\tau, q) = 1 + \beta\left[\exp\left(-\Gamma_1(q)\tau + \frac{\Gamma_2(q)}{2}\tau^2\right)\right]^2, \quad \text{(S2)}$$

where $\Gamma_1(q)$ and $\Gamma_2(q)$ are the 1-st and 2-nd order cumulants and β is the coherence factor. The hydrodynamic radius, R_H, was calculated using the Stokes-Einstein formula from the z-averaged translation diffusion coefficient, D, obtained from $\Gamma_1(q)/q^2$ values extrapolated to $q \to 0$ (Fig. S1, curve 2) as

$$\frac{\Gamma_2(q)}{q^2} = D(1 + R_g^2 C q^2), \quad \text{(S3)}$$

where C is the parameter dependent on the shape, dispersity and internal dynamics of the NPs.

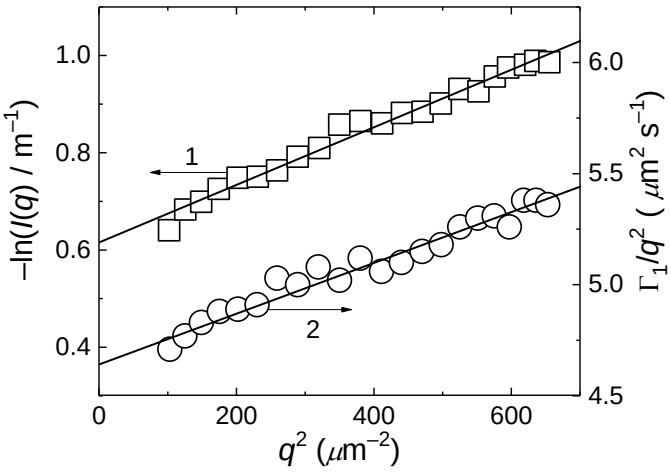

Figure S1. (a) Logarithm of the scattering intensity, $\ln(I(q))$ (curve 1), and the apparent diffusion coefficient, $\Gamma_1(q)/q^2$ (curve 2) as functions of q^2, from the SLS and DLS measurement of 0.15 mg ml^{-1} NPs dispersion.

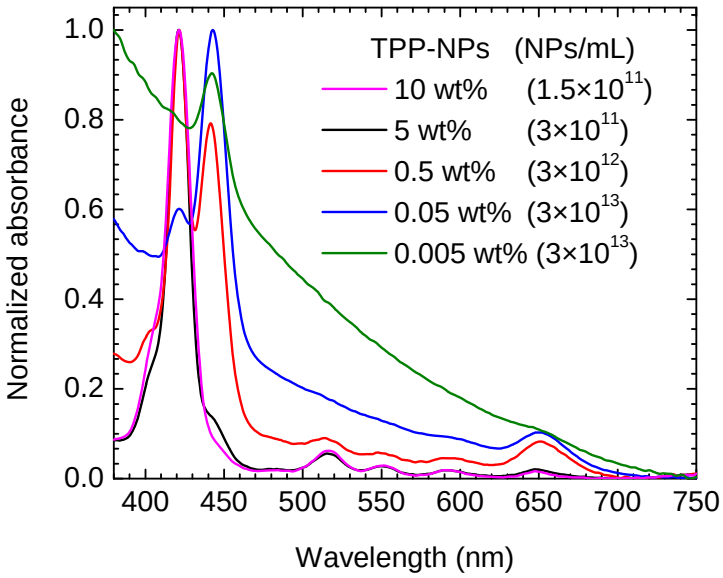

Figure S2. Normalized UV-Vis spectra of **TPP-NPs**. The dispersions have the same overall amount of TPP which was achieved by a different number of NPs.

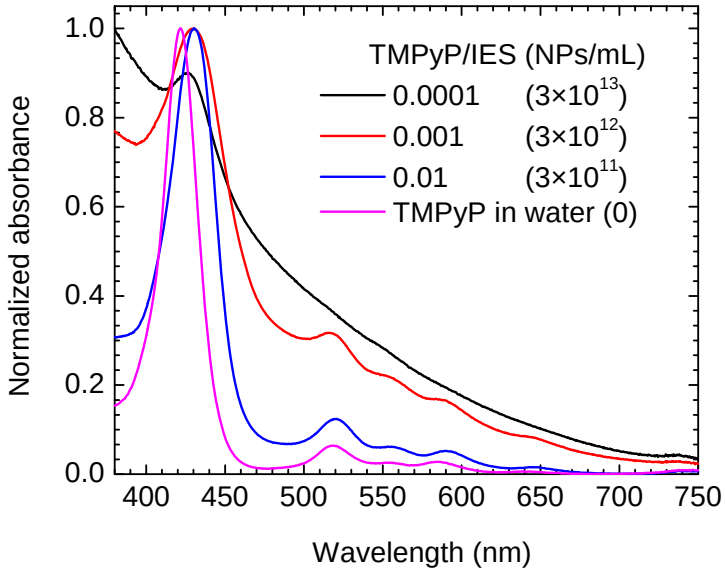

Figure S3. Normalized UV-Vis spectra of TMPyP and **TMPyP-NPs**. The dispersions have the same overall amount of TMPyP which was achieved by a different number of NPs.

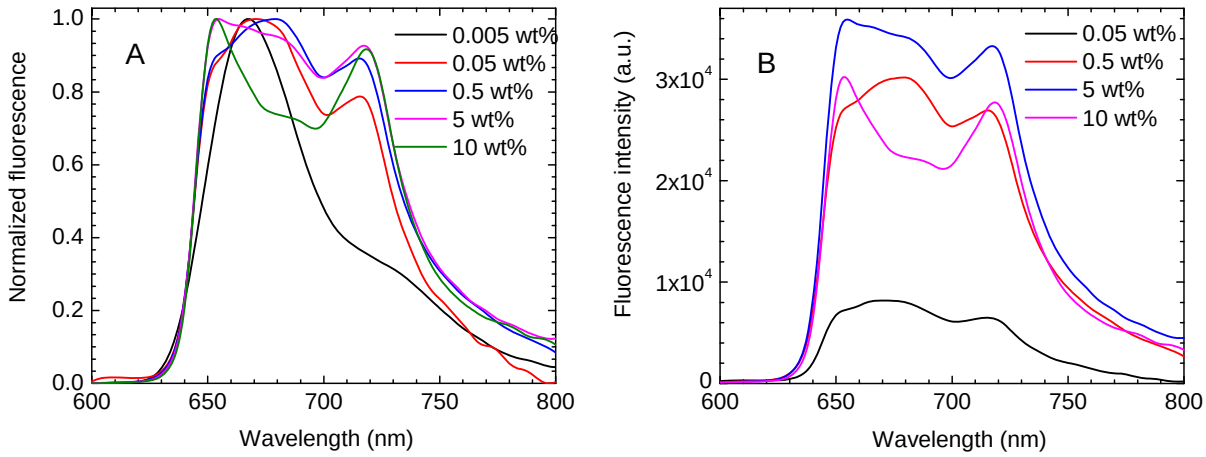

Figure S4. Normalized fluorescence emission spectra (A) and the same spectra in original intensities (B) of **TPP-NPs** dispersions. The samples have the same overall content of TPP (2×10^{-7} mol l^{-1}) which was achieved by a different number of NPs (1.5×10^{11} – 3×10^{13} NPs ml^{-1}). Excitation at λ_{exc} = 516 nm.

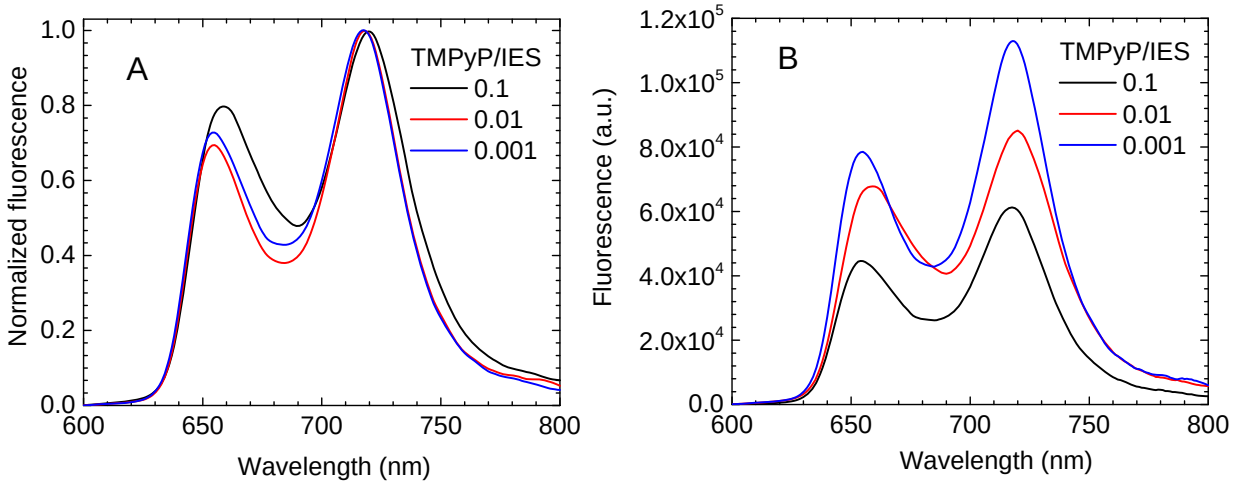

Figure S5. Normalized fluorescence emission spectra (A) and the same spectra in original intensities (B) of **TMPyP-NPs** dispersions. The samples have the same overall content of TMPyP (1×10^{-6} mol l^{-1}) which was achieved by a different number of NPs (1.5×10^{11} – 1.5×10^{13} NPs ml^{-1}). Excitation at λ_{exc} = 430 nm.

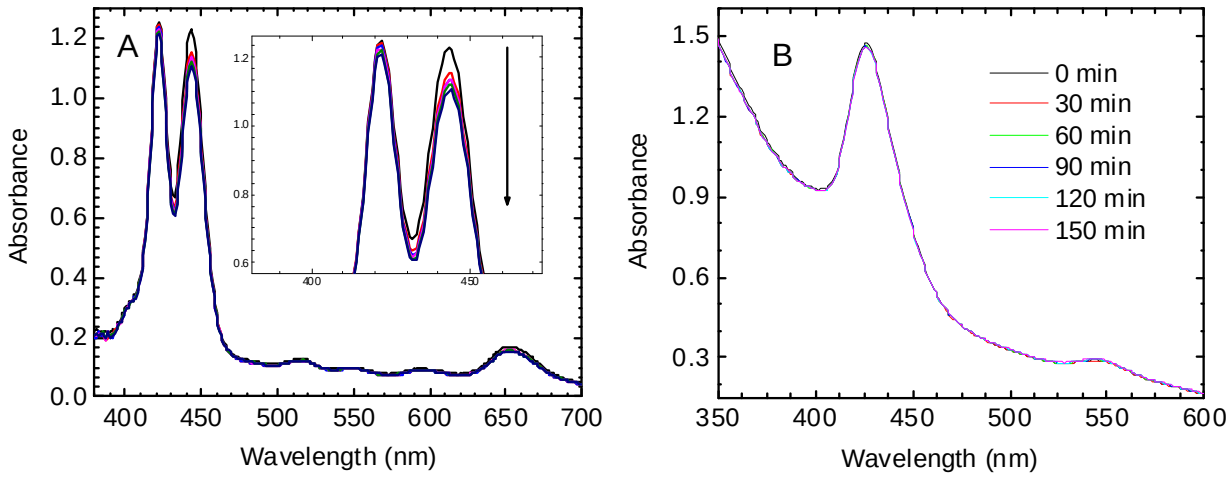

Figure S6. Photostability test: Photodegradation of **TPP-NPs** (0.5 wt%; panel A) and **TMPyP-NPs** (0.01 TMPyP/IEC; panel B) dispersions (1.5×10^{13} NPs ml^{-1}) during the irradiation by a 500 W xenon lamp equipped with a 400 nm long pass filter.

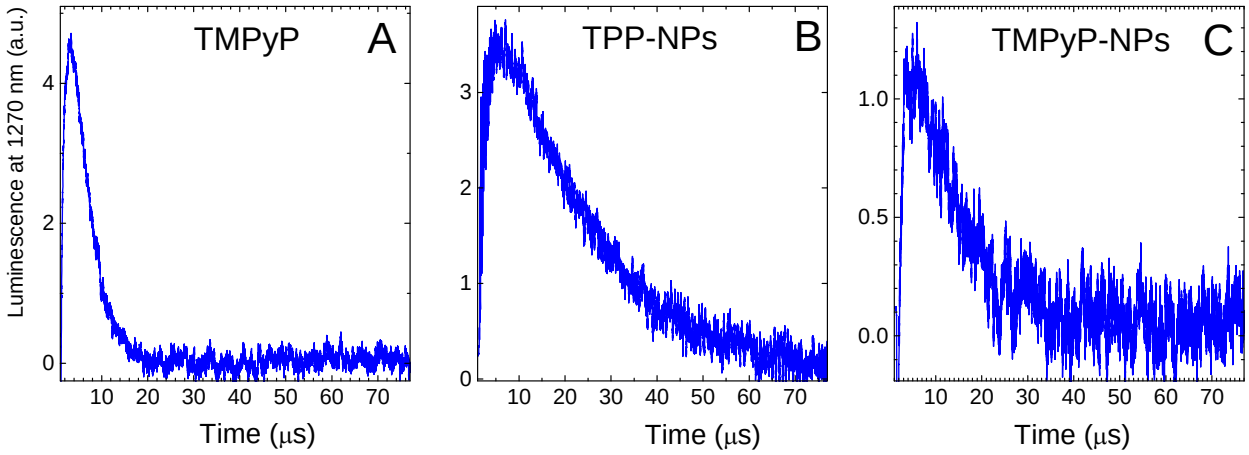

Figure S7. Kinetics of $O_2(^1\Delta_g)$ photogenerated by TMPyP in H_2O (τ_Δ ~ 3-4 μs) (A), **TPP-NPs** (B) and **TMPyP-NPs** (C). The kinetics of $O_2(^1\Delta_g)$ deactivation in **TPP-NPs** is controlled by the polymer (i.e., oxygen diffusion coefficient, number of quenching groups and the size of NPs) (B). The kinetics of $O_2(^1\Delta_g)$ produced by **TMPyP-NPs** is evidently affected by partial diffusion of $O_2(^1\Delta_g)$ through the polymer matrix having higher τ_Δ than water (C).

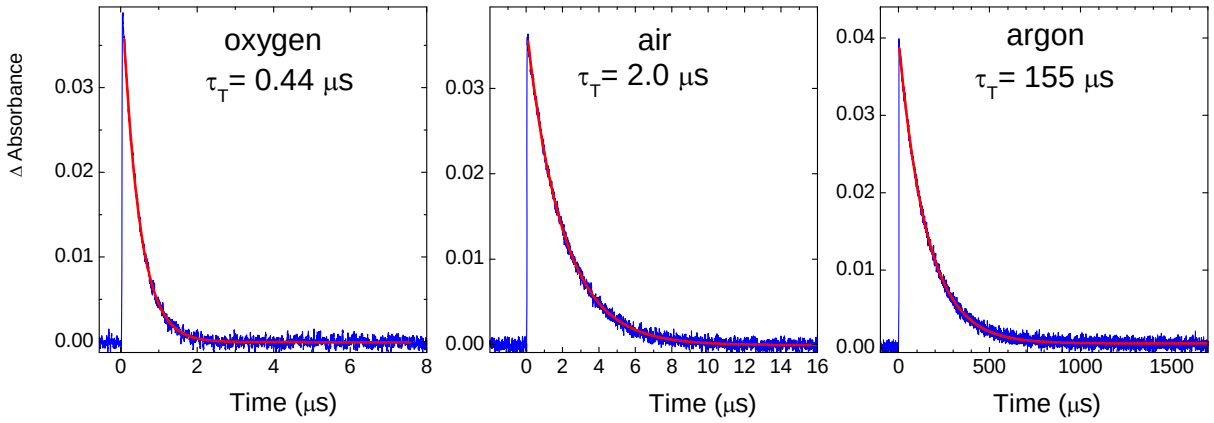

Figure S8. Kinetics of the triplet states of TMPyP in H_2O.

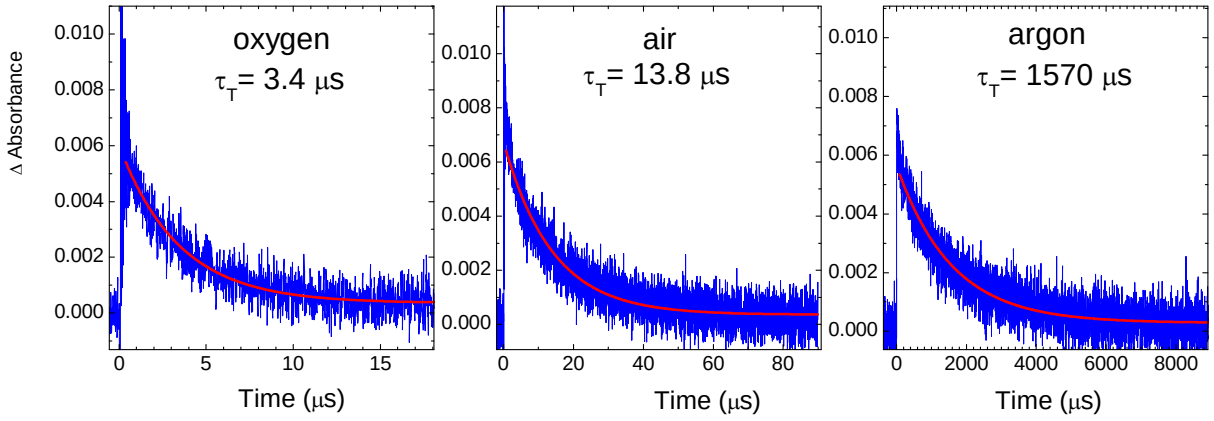

Figure S9. Kinetics of the triplet states of 0.5 wt% **TPP-NPs** in H_2O.

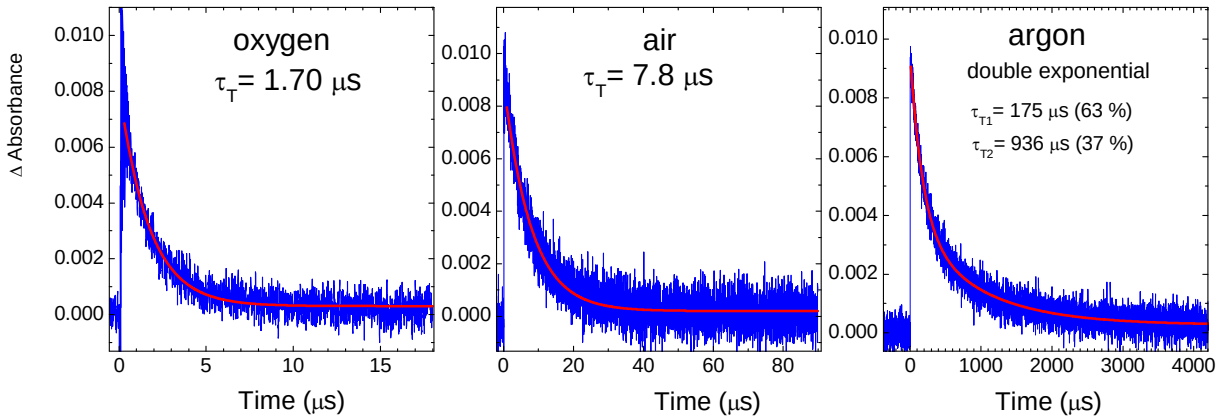

Figure S10. Kinetics of triplet states of **TMPyP-NPs** in oxygen-, air-, or argon-saturated H_2O. The traces were recorded at 460 nm upon excitation by a 425 nm laser pulse; red lines represent corresponding exponential fits.

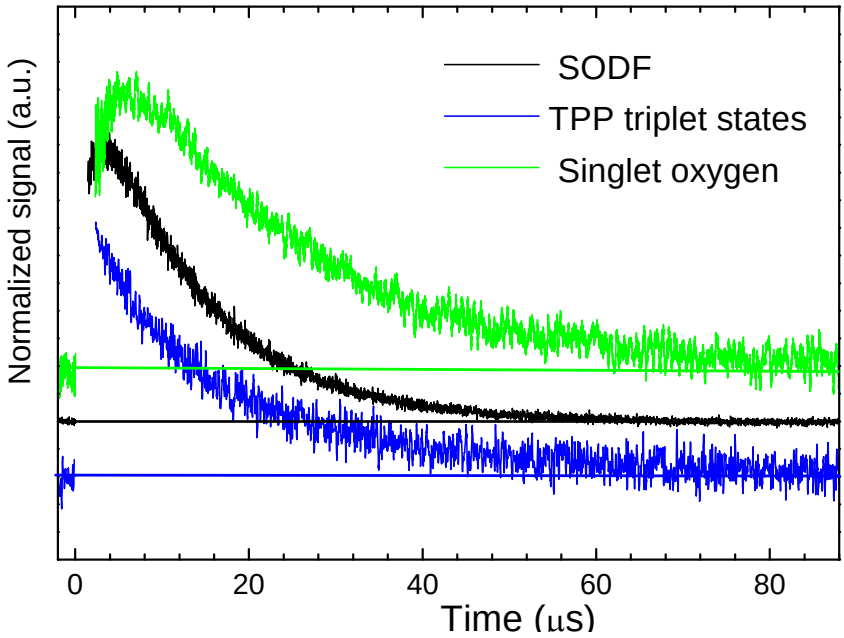

Figure S11. Kinetics of $O_2(^1\Delta_g)$, porphyrin triplet states and SODF in air-saturated 0.5 wt% **TPP-NPs** water dispersion.

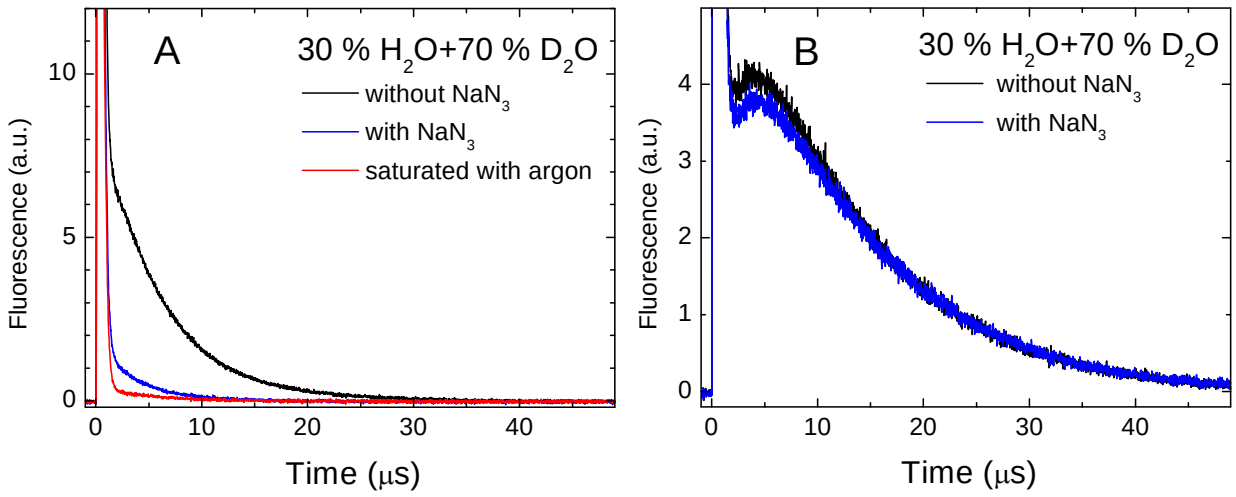

Figure S12. SODF of **TMPyP-NPs** (0.1 TMPyP/IES) (A) and 0.05 wt% **TPP-NPs** (B) in the presence and absence of a singlet oxygen quencher, NaN_3, in air-saturated D_2O/H_2O. The absence of SODF is documented by the measurement of **TMPyP-NPs** in oxygen-free D_2O/H_2O.

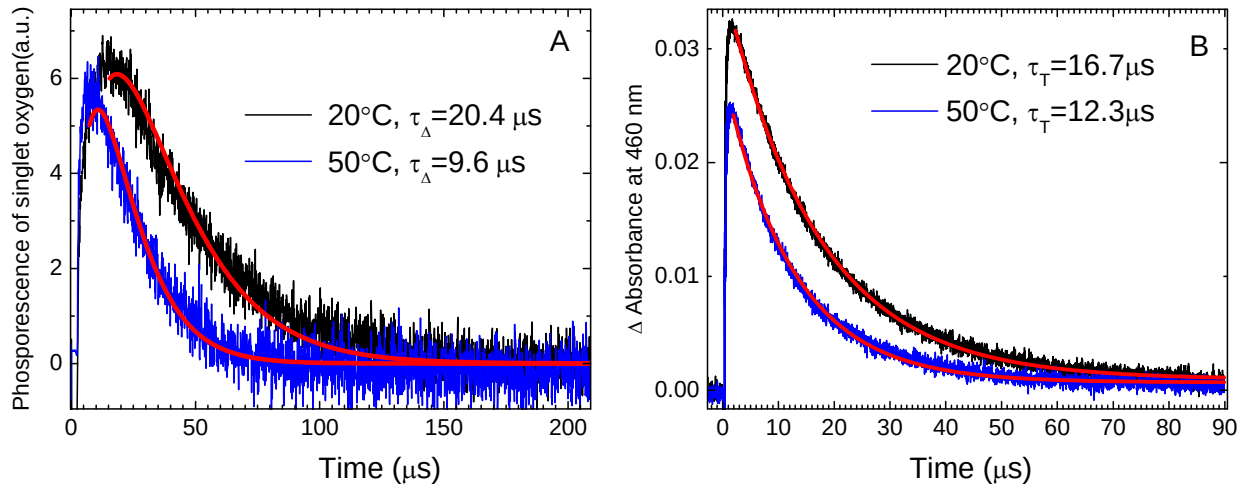

Figure S13. Temperature dependence of $O_2(^1\Delta_g)$ phosphorescence (A) and TPP triplet state (B) kinetics in the polystyrene nanofiber material containing 1 wt% TPP.

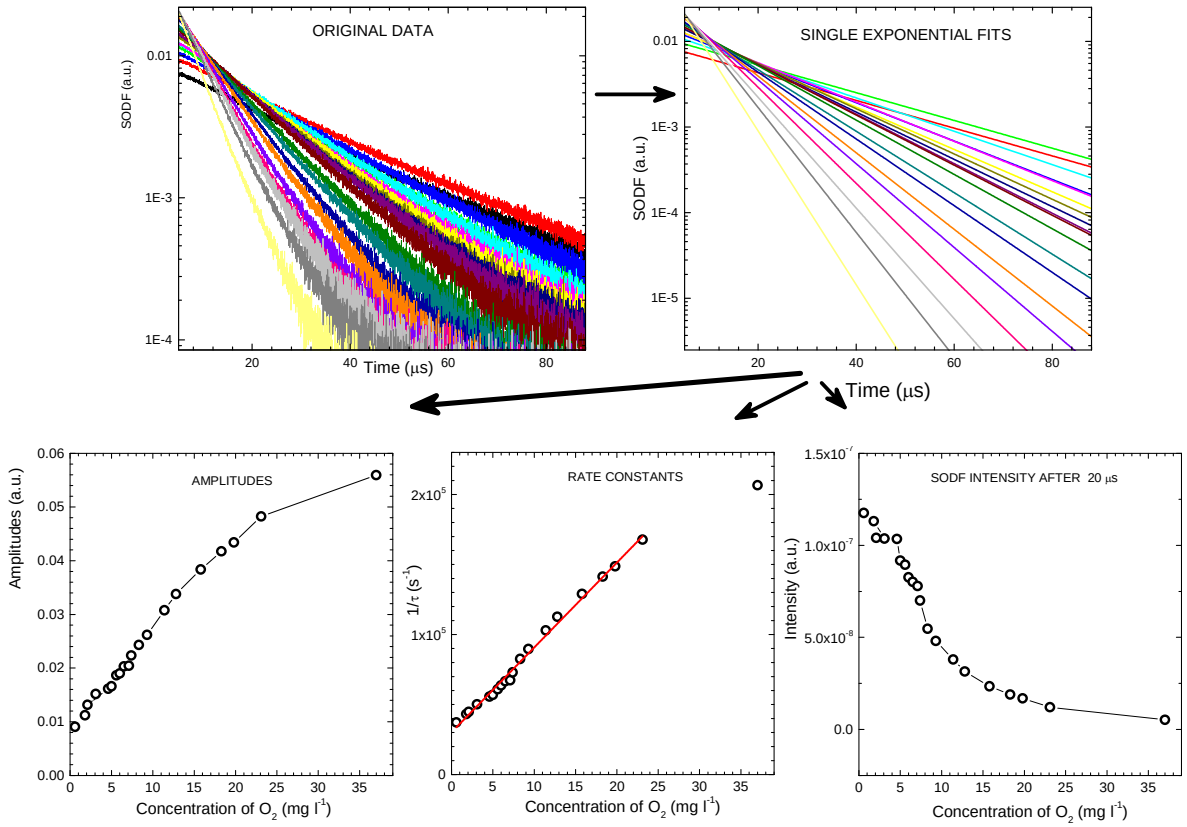

Figure S14. Dependence of SODF on dissolved oxygen concentration: amplitudes of exponential fits *vs*. oxygen concentration (left), the Stern-Volmer plot, i.e., $1/\tau_{SODF}$ *vs*. oxygen concentration (middle), and overall SODF intensity after 20 μs *vs*. oxygen concentration (right).

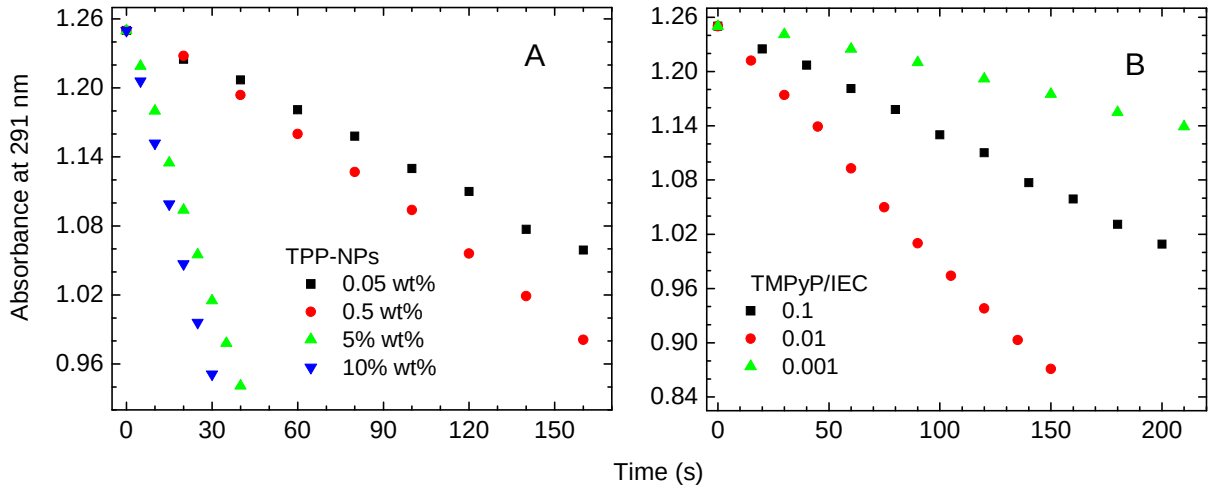

Figure S15. Photooxidation of uric acid by the **TPP-NPs** (A) or **TMPyP-NPs** (B) dispersions containing the same number of NPs (3×10^{11} NPs ml^{-1}) during continuous irradiation at 25°C. Irradiated by a 500 W Xe-lamp equipped with a long pass filter ($\lambda \geq 400$ nm), absorption of 3 ml of air-saturated 10^{-4} M uric acid was recorded at 291 nm.

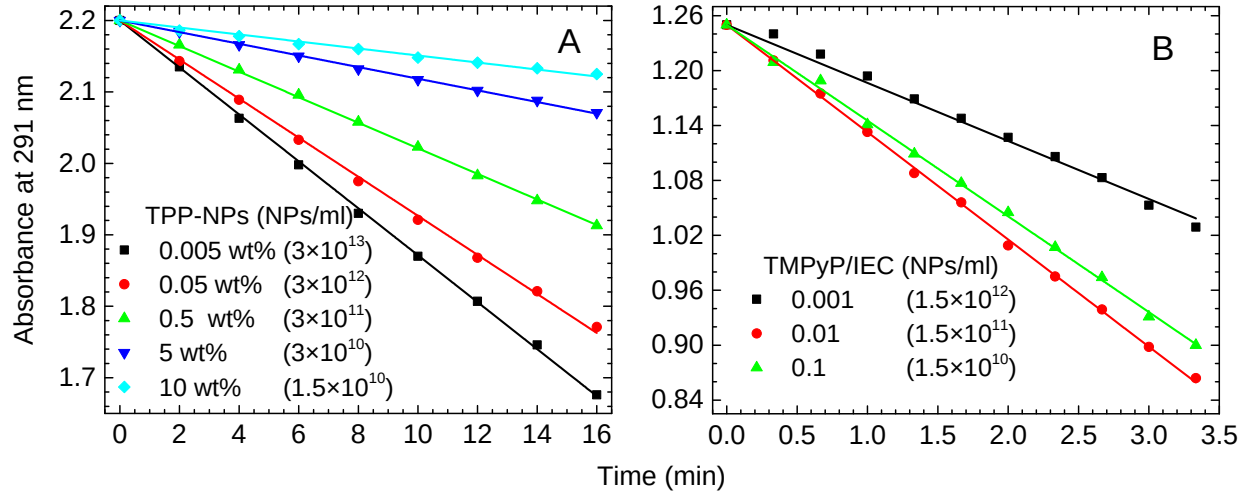

Figure S16. Photooxidation of uric acid by the **TPP-NPs** (A) or **TMPyP-NPs** (B) dispersions containing the same content of TPP (2.4×10^{-8} mol l^{-1}) or TMPyP (5.0×10^{-8} mol l^{-1}) achieved by the varying number of NPs. The experimental conditions are described above.

Table S1. Parameters of prepared sulfonated NPs, the case analysis.

Parameter	Description	Calculation / Note	
P1	Mass of NPs per ml (mg ml^{-1})	From the gravimetric measurement	3.2±0.2
P2	Mass of sulfonated nanofiber membrane (mg)	From the gravimetric measurement	154
P3	Volume of the stock dispersion (ml)	-	45
P4	Yield of NPs preparation	**P4 = (P1×P3)/P2**	94 %
P5	Molar mass of the NPs (g mol^{-1})	See Equation S1	6.8×10^{7}
P6	Avogadro's number (mol^{-1})	-	6.022×10^{23}
P7	Average radius of NPs (cm)	From TEM measuring	1.5×10^{-6}
P8	Surface of 1 NP (cm^2)	**P8** = 4π(**P7**)^2	2.8×10^{-11}
P9	Volume of 1 NP (cm^3)	**P9** = $4/3\pi$(**P7**)^3	1.4×10^{-17}
P10	Number of NPs per ml (in the stock dispersion)	**P10 = (P1/(P5**×1000))×**P6**	3×10^{13}
P11	Theoretical effective volume reached by $O_2(^1\Delta_g)$ in 1 ml of the stock dispersion (ml)	**P11 =P10×4/3π(r_{ef})^3** **r_{ef} = P7 + lr** Effective radius (**r_{ef}**) = average radius of NPs (**P7**) + effective range of $O_2(^1\Delta_g)$ (**l_r** = 20.5×10^{-6} cm)	1.3
P12	Average IEC of NPs (mol ml^{-1})	Determined by titration	1×10^{-6}
P13	Average IEC of NPs (mol g^{-1})		3×10^{-4}

Table S2. Parameters of prepared photoactive NPs: PE is the relative photo-oxidation efficacy of NPs towards uric acid (UA), calculated as the slope of $A(\text{UA})/\Sigma I_0(1\text{-}10^{-Ai})$ *vs*. irradiation time plot (Figure 11), where $\Sigma I_0\ (1\text{-}10^{-Ai})$ is the sum of absorbed light intensities at wavelengths λ_i (400-700 nm) and A(UA) is the absorbance of UA at 291 nm; Φ_F is the fluorescence quantum yields at indicated wavelength in parentheses.

Continuous irradiation was performed with a 500 W Xe-lamp equipped with a long pass filter ($\lambda \geq 400$ nm).

NPs		Average number of TPP molecules per NP	Slope $A(\text{UA})/\Sigma I_0(1\text{-}10^{-Ai})$	PE	Φ_F
TPP-NPs (wt %)	0.005	5	-0.0023	1	0.17 (443 nm)
	0.05	50	-0.0013	0.6	0.16 (443 nm)
	0.5	500	-0.0008	0.3	0.13 (443 nm) 0.10 (421 nm)
	5	5000	-0.0005	0.2	0.07 (421, 516 nm)
	10	10000	-0.0003	0.1	0.04 (421, 516 nm)
TMPyP-NPs (TMPyP/IES)	0.001	20	-0.0022	1	0.04 (428 nm)
	0.01	200	-0.0020	0.9	0.04 (428, 516 nm)
	0.1	2000	-0.0016	0.7	0.04 (428, 516 nm)

Table S3. Oxygen properties: $D(O_2)$ are the diffusion coefficients, c are the oxygen solubility in H_2O and τ_Δ are the $O_2(^1\Delta_g)$ lifetimes at indicated temperatures.

Temperature	$D(O_2)$ ($10^5 cm^2 s^{-1}$)		c (mg l^{-1})[c]	τ_Δ (μs)	
(°C)	H_2O[a]	Polystyrene[b]		H_2O[d]	Polystyrene[e]
5	1.1	-	12.6	3.6	21.7
10	1.2	0.009	11.1	-	20.3
20	1.8	0.014	8.8	3.5	17.2
37	2.6	0.030	6.6	-	-
50	3.3	0.049	5.7	3.3	10.4

[a]Han, P.; Bartels, D. M. Temperature Dependence of Oxygen Diffusion in H_2O and D_2O. *J. Phys. Chem.* **1996**, *100*, 5597-5602.

[b]Gao, Y.; Baca, A. M.; Wang, B.; Ogilby, P. R., Activation Barriers for Oxygen Diffusion in Polystyrene and Polycarbonate Glasses: Effects of Low Molecular Weight Additives. *Macromolecules* **1994**, *27*, 7041-7048.

[c] Measured by InPro 6880i oxygen sensor (Mettler Toledo).

[d]Jensen, R. L.; Arnbjerg, J.; Ogilby, P. R. Temperature Effects on the Solvent-Dependent Deactivation of Singlet Oxygen. *J. Am. Chem. Soc.* **2010**, *132*, 8098-8105.

[e]Calculated using data in Suchánek, J.; Henke, P.; Mosinger, J.; Zelinger, Z.; Kubát, P., Effect of Temperature on Photophysical Properties of Polymeric Nanofiber Materials with Porphyrin Photosensitizers. *J. Phys. Chem. B* **2014**, *118*, 6167-6174.